

Resonant tunneling in graphene-ferroelectric-graphene junctions

David Koprivica¹ and Eran Sela¹

¹*Raymond and Beverly Sackler School of Physics and Astronomy, Tel-Aviv University, IL-69978 Tel Aviv, Israel*
(Dated: October 3, 2022)

We study tunnel junctions consisting of a two-dimensional ferroelectric material sandwiched between graphene electrodes. We formulate a theory for the interplay of the polarization and induced free charges in such devices, taking into account quantum capacitance effects. We predict a gate sensitive voltage difference across the polar domains, which can be measured using electrostatic force microscopy. Incorporating this electrostatic theory in the tunneling current-voltage characteristics, we identify a resonance peak associated with aligned Dirac cones as a highly sensitive probe of the polarization. This opens the way for device applications with few atom-thick polar layers acting as readable ultra-high-density memory.

I. INTRODUCTION

Recent breakthroughs in two-dimensional (2D) van der Waals materials led to the experimental realization of a new form of ferroelectricity (FE)¹⁻⁶. This newly discovered interfacial ferroelectricity results from polar stacking configurations that break inversion symmetry, such as in AB or BA stacked hexagonal boron nitride (h-BN) bilayer^{2,3} or other 2D materials⁴⁻⁶. Remarkably, the resulting polarization can be flipped³ by a relative sliding of the layers by a single atomic distance.

Understanding the response to electric fields and the nature of ferroelectricity^{7,8} in these experiments requires further study and a possible distinction of these various systems⁹. In the bulk of twisted interfaces there is a Moiré-triangular lattice of alternating AB and BA regions which expand or shrink at finite field⁵. Yet, *in average* over many Moiré unit cells there is no remnant polarization at zero field¹⁰. On the other hand, in Refs. 2 and 3 hysteresis was seen, and specifically in Ref. 3, the flipping of a polar domain was attributed to the sliding of a domain wall near the edge of the bilayer, rather than in the bulk⁹. Leaving the precise sliding FE mechanism aside, here we shall be concerned only with uniform AB and BA polar interfaces.

Ferroelectric tunnel junctions, consisting of a thin FE material sandwiched between two electrodes, permit reading the polarization via tunnelling electroresistance (TER)¹¹⁻¹⁵. What is the fate of interfacial polarization within a tunnel junction?

In this work, we theoretically study 2D tunnel junctions consisting of uniform AB or BA polar interfaces sandwiched by graphene electrodes, as shown in Fig. 1(a). Assuming a given value for the bare polarization $V_P^{(0)}$, which, in principle, can be determined by *ab initio* methods, we focus on the interplay of the polarization and screening charges forming on the graphene electrodes. Related questions were recently addressed within density functional theory (DFT)¹⁶, where it was found that whereas metallic electrodes significantly affect the polarization of a bilayer h-BN, adding graphene spacers between the FE and metals restores the polarization and results in a significant TER. Here, we provide a phe-

nomenological electrostatic model. We find that when one of the electrode's Fermi level is tuned to the Dirac point, the electronic equilibration is dominated by quantum capacitance, and then a polar domain associated local voltage can be measured across the device.

We focus on basic mechanisms allowing to read out the polarization direction and magnitude from the current-voltage characteristics. One TER mechanism results from the dependence of the electrostatic tunneling barrier on the polarization orientation. We discuss a model allowing to estimate this barrier modulation in the 2D limit.

Moreover, a graphene-FE-graphene junction allows for a more sensitive finite voltage TER mechanism due to 2D momentum conservation. Resonance tunneling peaks in the $I(V)$ characteristics were identified both in planar 2D junctions of semiconductor heterostructures^{17,18}, and more recently in 2D materials¹⁹⁻²¹, specifically for graphene-h-BN-graphene¹⁹. There, the h-BN material simply acts as a barrier^{15,22,23}, whereas the resonance peaks emerge due to momentum conserving tunneling between the graphene electrodes. The device we consider is almost the same as in Ref. 19, where now the barrier consists of a parallel stacked h-BN bilayer supporting the polar AB or BA interfaces. Such a device is expected to be a perfect candidate to employ resonance tunneling peaks as a sensitive probe of interfacial polarization, which essentially acts as an internal voltage that shifts the resonance. We indeed find using our self-consistent model a sizable shift of the resonance peak¹⁹⁻²¹ for the two polarization directions.

The paper is organized as follows. After introducing the model in Sec. II, we study the Kelvin probe voltage in Sec. III. In Sec. IV we estimate the ratio of the tunneling coefficients in our device. In Sec. V we consider momentum conserving tunneling and focus on resonance peaks as a means to detect the polarization. We summarize in Sec. VI.

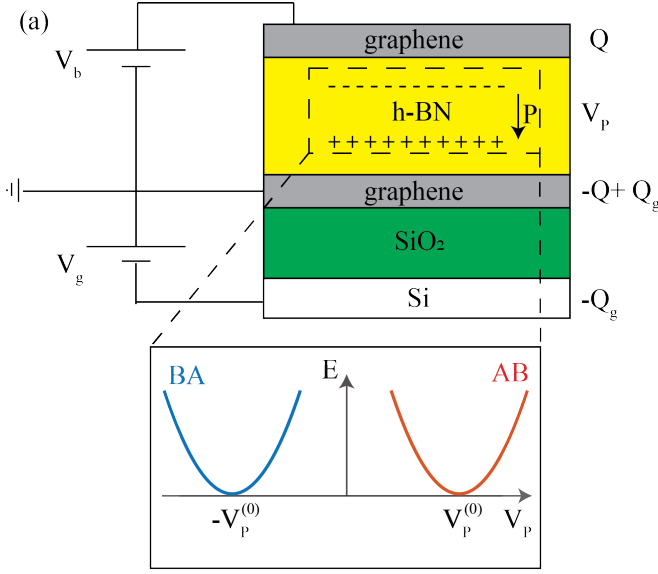


FIG. 1. (a) FE tunnel junction: a pair of tunnel coupled graphene sheets and a bottom gate are modeled by a pair of plate capacitors C_0, C_g . The polar bilayer interface is stacked inside the graphene-graphene capacitor and leads to an internal voltage denoted V_P . (b) Schematic free energy of the polarization of the interface, V_P . The system consists of two degenerate minima corresponding to stacking configurations AB and BA. In our model Eq. (1) the polarization, V_P , which takes the value $V_P^{(0)}$ for the bare bilayer, interacts with the electric field due to the electrons in the graphene sheets and gate.

II. MODEL

As shown in Fig. 1(a), we consider a tunneling junction consisting of a 2D polar interface encapsulated between two graphene sheets. Our theory is not restricted to a specific material, but for definiteness we consider parallel stacked bi-layer h-BN, having two polar stacking configurations denoted AB and BA exhibiting a finite out of plane polarization P which is accounted for by an internal voltage denoted V_P , see Fig. 1(b). A tunneling current is enabled by a bias voltage V_b . The bottom graphene sheet is gated by a voltage V_g . The energy describing the system is given by

$$\begin{aligned}
 E(Q, Q_g, V_P) = & \frac{Q^2}{2C_0} - Q(V_b + V_P) \\
 & + \frac{Q_g^2}{2C_g} - Q_g V_g \\
 & + \frac{C_0}{2} \frac{\epsilon_r}{\epsilon_r - 1} (V_P - pV_P^{(0)})^2 \\
 & + E_G(Q) + E_G(-Q + Q_g). \quad (1)
 \end{aligned}$$

Here C_0 is the capacitance between the two graphene sheets, and C_g is the capacitance between the bottom graphene sheet and a gate. We measure energy, charge and capacitance per unit area.

The third line encapsulates a quadratic expansion of the free energy³ around the minima for either one of the two stacking configurations denoted by $p = \pm 1$. By construction, the bare KP voltage (i.e. without the electrodes) is given by $\pm V_P^{(0)}$ for AB or BA stacking, see Fig. 1(b). Its value $V_P^{(0)} \approx 120\text{mV}$ was measured directly using Kelvin probe force microscopy³. In addition, this term renormalizes the capacitance $C_0 \rightarrow C = C_0 \epsilon_r$ by the dielectric constant of the material.

The last line represents the quantum capacitance of the graphene sheets, with

$$E_G(Q) = \frac{2}{3} \beta |Q|^{\frac{3}{2}}, \quad (2)$$

and $\beta = \sqrt{\frac{\pi}{e^3}} \hbar v_F$. $E_G(Q)$ is the total kinetic energy density measured from the Dirac point, valid in the vicinity of the Dirac point, and $Q > 0 (Q < 0)$ refers to holes (electrons).

The goal of this electrostatic model is to allow variations of the polarization of the AB or BA interface due to electric fields produced by the graphene electrodes.

The equilibrium configuration is obtained by minimizing the energy with respect to the charge induced on the top sheet Q and on the gate Q_g , and the polarization of the interface V_P . The equation $\frac{\partial E}{\partial V_P} = 0$ gives

$$V_P = pV_P^{(0)} + \frac{(\epsilon_r - 1)Q}{\epsilon_r C_0}, \quad (3)$$

showing that the internal polarization is affected by the electrodes. Defining the Fermi energy

$$E_F(Q) = -e \frac{\partial E_G(Q)}{\partial Q} = -e \text{sign}(Q) \beta |Q|^{1/2}, \quad (e > 0), \quad (4)$$

the equations $\frac{\partial E}{\partial Q} = \frac{\partial E}{\partial Q_g} = 0$ yield

$$0 = \frac{Q}{C} - V_b - pV_P^{(0)} - E_F(Q)/e + E_F(Q_g - Q)/e, \quad (5)$$

$$0 = \frac{Q_g}{C_g} - V_g - E_F(Q_g - Q)/e. \quad (6)$$

Eqs. (5) and (6) are subsequently solved numerically for Q and Q_g as function of V_g and V_b for either sign of the polarization $p = \pm 1$.

III. KELVIN PROBE VOLTAGE

In this section we calculate the KP voltage, which can be measured via scanning atomic force microscopy (AFM) as function of gate and bias voltages, in a setup as in Fig. 2(a). Such measurements were performed for the bare ferroelectric material²⁻⁴. Our theory addresses the renormalization of the internal polarization V_P and the resulting total KP voltage V_{KP} across the electrodes.

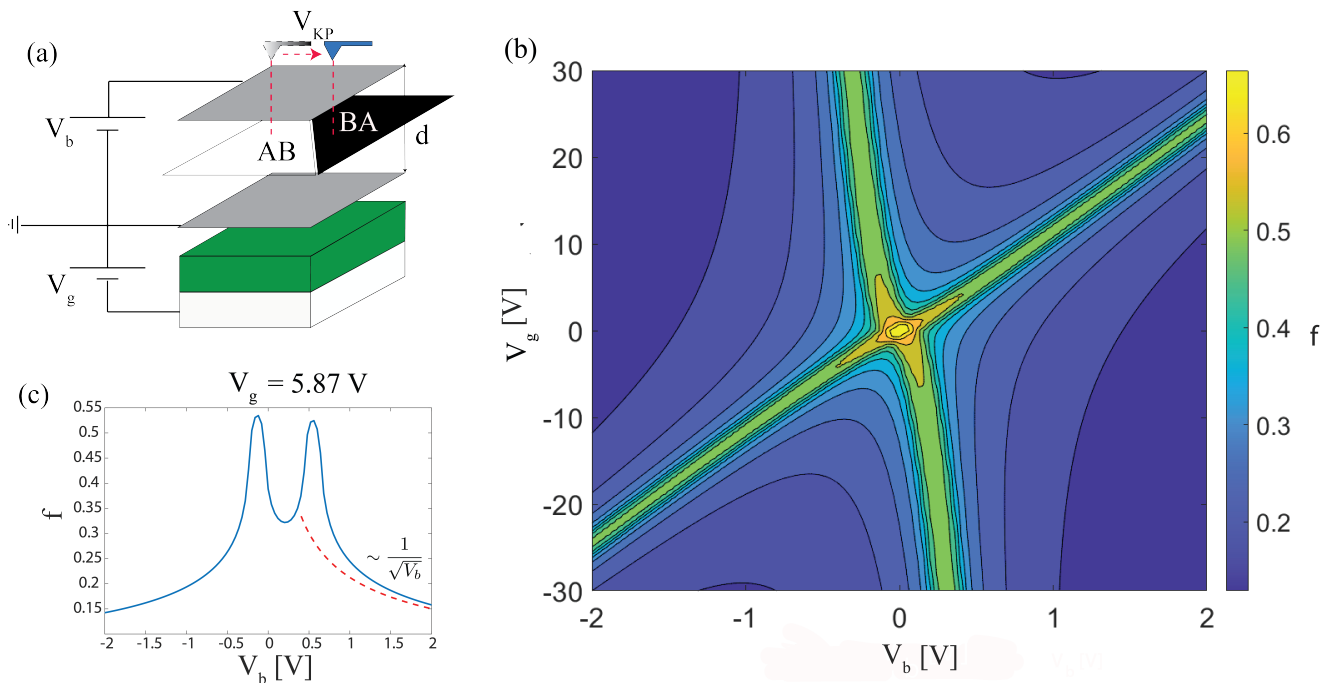


FIG. 2. (a) Schematic view of the Kelvin probe measurement device. We define the Kelvin probe sensitivity (KPS) $f = \delta V_{KP}/(2V_P^{(0)})$ [see Eq. (8)] as the relative difference in the voltage measured for the two polarization orientations of the two stacking configurations AB and BA . (b) KPS versus gate and bias voltage. Maximal sensitivity occurs when one of the graphene sheets is at charge neutrality. (c) Cut along a fixed gate voltage showing a double peak. A fit (dashed line) to Eq. (10) shows that the KPS decays at large bias as $V_b^{-\frac{1}{2}}$. In this and all subsequent calculations we use $d = 5\text{nm}$, $d_g = 90\text{nm}$ (width of gate capacitor) and $\epsilon_r = 3.8$.

The total voltage drop measured in a Kelvin probe setup as in Fig. 2(a) is given by

$$V_{KP} \equiv V_P - \frac{Q}{C_0} = pV_P^{(0)} - \frac{Q}{C}, \quad (7)$$

where we used Eq. (3). We subsequently focus on the difference of V_{KP} for the two polarization orientations, $\Delta V_{KP} = V_{KP}^{(+)} - V_{KP}^{(-)}$ which can be measured by scanning the AFM tip across a stacking domain wall, see Fig. 2(a).

It is convenient to measure ΔV_{KP} in units of the bare polar domains voltage by defining the Kelvin probe sensitivity (KPS)

$$f \equiv \frac{\Delta V_{KP}}{2V_P^{(0)}} = 1 - \frac{Q^+ - Q^-}{2CV_P^{(0)}}. \quad (8)$$

The second equality, obtained from Eq. (7), shows that $f \rightarrow 1$ in the absence of charges on the electrodes.

The numerical solution for ΔV_{KP} and hence the KPS is shown in Fig. 2(b) as function of bias and gate voltages. A cut with fixed V_b is shown in Fig. 2(c). We can see that ΔV_{KP} peaks when either one of the two graphene sheets is at charge neutrality and takes a value which is of the order of $V_P^{(0)}$ (and hence $f \lesssim 1$). Along these peaks the charge transfer between the electrodes is small and primarily determined by quantum capacitance, and hence

it very inefficiently screens electrostatically the internal polarization.

We now discuss the physics describing the tail and peaks of ΔV_{KP} (or equivalently f in Fig. 2(c)). The tails can be analysed by considering the quantum capacitance as a small perturbation. One can solve Eqs. (5) and (6) up to a given order in β . In the absence of quantum capacitance ($\beta \rightarrow 0$) we have

$$Q \rightarrow Q^{(0)} \equiv C(V_b \pm V_P^{(0)}), \quad Q_g \rightarrow Q_g^{(0)} \equiv C_g V_g. \quad (9)$$

Then $V_{KP}^{\pm} = V_b$, $\Delta V_{KP} = 0$, and $f \rightarrow 0$. The vanishing KPS is expected since the potential on the electrodes adjusts such as to completely screen the internal polarization. Considering a small quantum capacitance correction, $Q = Q^{(0)} + \delta Q$, $Q_g = Q_g^{(0)} + \delta Q_g$, and expanding Eq. (5) to linear order in these deviations, we obtain for $V_b \gg V_P^{(0)}$

$$f \rightarrow \beta \sqrt{\frac{C}{V_b}}. \quad (10)$$

This is confirmed as a dashed line in Fig. 2(c).

The height of the two peaks in Fig. 2(c) can be obtained by considering the quantum capacitance of the corresponding neutralized graphene sheet as the dominant term. Consider for example the $Q = 0$ peak [nearly

vertical peak ridge in Fig. 2(b)]. We can then decouple Eqs. (5) and (6) by replacing the Fermi energy of the bottom layer $E_F(Q_g - Q)$ by $E_F(Q_g)$. We thus obtain $0 = \frac{Q}{C} - V_b - pV_P^{(0)} - E_F(Q)/e + E_F(Q_g)/e$, yielding a peak at $V_b = E_F(Q_g)/e$ where for large V_g we have $Q_g = C_g V_g$. Solving the quadratic equation yields $Q = p \left(-C\beta + \sqrt{(C\beta)^2 + 4CV_P^{(0)}} \right)^2 / 4$. Substituting in Eq. (8), we have $f = 1 - \frac{Q}{CV_P^{(0)}}$. Expanding in small $V_P^{(0)}$, yields

$$f = 1 - \frac{V_P^{(0)}}{C\beta^2} + \mathcal{O}((V_P^{(0)})^2). \quad (11)$$

We can see that $C\beta^2$ sets a voltage scale below which quantum capacitance effects set in. In our system

$$\mathcal{V} \equiv C\beta^2 = \frac{e}{16\pi d\epsilon_0} \left(\frac{4\pi\epsilon_0\hbar v_F}{e^2} \right)^2 \sim 0.3V. \quad (12)$$

Thus, the reason that the peaks in KPS approach nearly unity is that the material property $V_P^{(0)}$ is small, but of the order of \mathcal{V} .

IV. POLARIZATION DEPENDENT TUNNELING COEFFICIENT

In this section we discuss the influence of the polarization on the tunneling coefficient $|\mathcal{T}|^2$. This effect can be understood from a polarization-dependent distortion of the electrostatic tunnel barrier^{24,25}, modifying the tunneling coefficient due to its exponential sensitivity $|\mathcal{T}|^2 \propto e^{-2\kappa d}$.

Let us denote the tunneling amplitudes for the two polarization orientations by \mathcal{T}^\pm and define the relative barrier modulation

$$\eta = \frac{|\mathcal{T}^+|^2 - |\mathcal{T}^-|^2}{|\mathcal{T}^+|^2 + |\mathcal{T}^-|^2}. \quad (13)$$

As a simple model providing an order of magnitude estimate for η , consider the bottom and top graphene sheets to be located at the $z = \pm d/2$ planes, and the two h-BN layers at the $z = \pm d/6$ planes. The tunneling amplitude from bottom to top is given via 3-rd order perturbation theory by²⁶ $\mathcal{T} \propto \frac{t^3}{E(z=-d/6)E(z=d/6)}$, where t are nearest layer hopping amplitudes, and $E(z = \pm d/6)$ is the energy in the h-BN layers. We denote by E_g the energy gap of the bare h-BN layer at $Q = 0$. Adding the linear potential due to the charged electrodes, $E(z) = E_g + \frac{eQz}{dC}$. The tunneling amplitude becomes $\mathcal{T}^\pm \propto \left(E_g^2 - \left(\frac{eQ^\pm}{6C} \right)^2 \right)^{-1}$.

If the two directions of polarization lead to exactly opposite charge transfer, $Q^+ = -Q^-$, then $\mathcal{T}^+ = \mathcal{T}^-$. In general $\eta = 0$ when inversion symmetry holds, namely

when $V_b = 0$ and $V_g = 0$. Finite barrier modulation results from $Q^+ \neq -Q^-$,

$$\eta \approx \frac{\left(\frac{eQ^-}{6C} \right)^2 - \left(\frac{eQ^+}{6C} \right)^2}{2E_g^2}. \quad (14)$$

For sufficiently large V_b , using Eq. (9) which ignores quantum capacitance effects, we have $\eta = -e^2 V_b V_P^{(0)} / (18E_g^2)$ independently of V_g . Assuming $E_g \sim 1eV$, this result leads to a few percent relative barrier modulation for a bias V_b of few volts. The smallness of the effect derives from the small ratio between the voltage $V_P^{(0)}$ and the gap of h-BN, however this can be made larger in other materials. Higher η may also be obtained in an asymmetric device when one electrode is weakly coupled while the other one is strongly coupled²⁷.

We note that the TER is defined [see Eq. (18) below and Refs. 13–15] in terms of the currents at finite bias voltage. Our definition of the relative barrier modulation in Eq. (13) allows to separate the effect of the modulation of the barrier itself, which leads to a relatively weak contribution to TER, from the effects associated with momentum conserving tunneling between two graphene sheets, to be considered in the next section.

V. MOMENTUM CONSERVING TUNNELING

In this section we consider 2D momentum conserving tunneling through the polar interface. In conventional tunnel junctions 2D momentum conservation leads to a resonance peak in the $I(V)$ characteristics corresponding to two aligned Dirac cones^{19–21}. Our goal is to incorporate the interfacial polarization into the resonant condition, yielding a sensitive probe of the polarization orientation and magnitude.

Following the model outlined in Ref. 19, we start with a Fermi golden rule expression for the tunneling current

$$I^{(\pm)} = |\mathcal{T}^\pm|^2 \sum_{\nu_B, \nu_T} \int d^2 k_T \int d^2 k_B \left(f_B(\varepsilon_{\vec{k}_B, \nu_B}) - f_T(\varepsilon_{\vec{k}_T, \nu_T}) \right) (V_q(k_B, k_T))^2 \delta \left(\varepsilon_{\vec{k}_B, \nu_B} - \varepsilon_{\vec{k}_T, \nu_T} - eV_{KP} \right). \quad (15)$$

In this section, in order to disentangle the TER effects of the previous chapter with effects of momentum conservation, we assume for simplicity $\mathcal{T}^+ = \mathcal{T}^-$. Here, $f_i(\varepsilon) = (\exp[(\varepsilon - E_{F,i})/T] + 1)^{-1}$ are Fermi functions and $\varepsilon_{\vec{k}_i, \nu_i} = \hbar v_F \nu_i |\vec{k}_i|$ are the electron ($\nu = 1$) and hole ($\nu = -1$) bands in the bottom or top sheet ($i = B, T$), respectively (see Fig. 3). This process describes tunneling of an electron from an occupied momentum state \vec{k}_B in the bottom layer to an unoccupied state with momentum \vec{k}_T at the top layer, measured from the respective Dirac point in a given valley. The scattering potential contains a phenomenological momentum dependence $V_q(k_B, k_T) = \frac{1}{q_B^2 + (\vec{k}_B - \vec{k}_T - \vec{Q})^2}$. Here $|\vec{Q}| = K\theta$ is

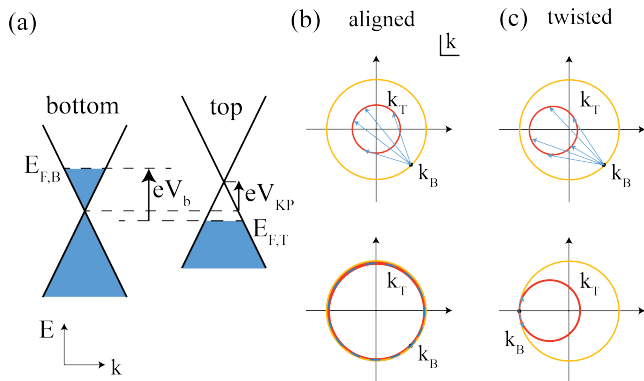


FIG. 3. (a) Typical energy band diagram (momentum shift for clarity). The Fermi levels of the bottom and top layers $E_{F,i}$ ($i = B, T$) are determined from the charge densities Q, Q_g . The KP voltage V_{KP} sets the energy misalignment of the Dirac points. (b) At zero relative twist angle equi-energy contours are concentric circles. At $V_{KP} = 0$ these rings exactly overlap for all energies (see marked energy diagram in Fig. 4), leading to a resonant momentum conserving tunneling in the entire voltage window between the two Fermi energies. (c) For finite twist the equi-energy circles are non-concentric, and resonance peaks occur when these circles are tangential for all energies (see marked energy diagrams in Fig. 5), when $eV_{KP} = \pm\Delta$ is satisfied (see Eq. (19)).

a momentum shift between the top and bottom Dirac points (at momentum K in the Brillouin zone) due to a relative twist of the layers by angle θ . The limit $q_c \rightarrow 0$ corresponds to momentum conserving tunneling. A finite q_c phenomenologically describes non-momentum-conserving tunneling processes e.g. due to short-range disorder or the Moiré pattern of either the h-BN or its interface with graphene. We take $q_c^{-1} = 12nm$ ¹⁹. The typical energy band diagram in the presence of a bias voltage is shown in Fig. 3(a). Since $E_{F,T} = E_F(Q)$ and $E_{F,B} = E_F(Q_g - Q)$ mark the distance of these Fermi levels from the corresponding Dirac point; from Eq. (5) it follows that the energy difference of the two Dirac points is given precisely by eV_{KP} , as marked in Fig. 3(a).

A. Zero twist angle

When the two graphene sheets are perfectly aligned we have $\vec{Q} = 0$. For any energy within the voltage window, the two momenta \vec{k}_B and \vec{k}_T belong to two concentric circles in momentum space, as denoted in Fig. 3(b). The energy displacement of the Dirac cones, eV_{KP} , is controlled by the bias voltage. When $V_{KP} = 0$ these two circles in momentum space overlap, for all energies, leading to a resonant current peak.

The resonance peak can be obtained by performing the

angular integration, leading to

$$I^{(\pm)} \propto \int_{-\infty}^{\infty} dk_T dk_B \frac{(f_B - f_T) |k_B| |k_T| (q_c^2 + k_B^2 + k_T^2)}{(q_c^2 + (k_B - k_T)^2)^{\frac{3}{2}} (q_c^2 + (k_B + k_T)^2)^{\frac{3}{2}}} \delta(\hbar v_F (k_B - k_T) - eV_{KP}). \quad (16)$$

This yields a single integral that we evaluate numerically.

Fig. 4 shows a color map of the current I versus V_b and V_g for a specific polarization direction. As a guide to the eye, this figure displays the charge neutrality curves of either bottom or top graphene sheets. We also plot the curve where $V_{KP} = 0$. A cut of the $I(V_b)$ curve for either direction of the polarization for fixed V_g is shown in the right-top inset of Fig. 4. We can see a pronounced resonance peak positioned precisely at V_b at which $V_{KP} = 0$ where the Dirac cones overlap. This occurs for different resonant voltages for the two polarization orientations.

The line shape of the peak versus V_b stems from the implicit dependence of V_{KP} on the latter, and takes the form

$$I(V_b)|_{V_{KP} \approx 0} \propto ((\hbar v_F q_c)^2 + (eV_{KP})^2)^{-3/2}. \quad (17)$$

We can also observe a plateau in the $I(V_b)$ curve in Fig. 4 which terminates at $V_b \approx 0.4V$ (at point 5). As shown in the energy diagrams in Fig. 4, this corresponds to a threshold for transport through the midway energy between the two Dirac points, see green dashed lines. At the threshold $V_b \approx 0.4V$ this specific energy enters into the voltage window²⁸.

We note that the shifted resonance peaks lead to a significant TER^{15,22,29}, defined as

$$\text{TER} = \frac{|I^{(+)} - I^{(-)}|}{\min(|I^{(+)}|, |I^{(-)}|)}, \quad (18)$$

as shown in Fig. 4 (right-bottom inset). The role of our definition of the relative barrier modulation η in Sec. IV meant to separate this effect from the modification of the tunneling amplitudes for the two polarization directions.

B. Finite twist angle

Tunneling between twisted graphene sheets has been discussed in numerous theory^{28,30} and experimental²⁰ works. Whereas at zero twist, there is a single resonance condition $V_{KP} = 0$ at which the two Dirac cones completely overlap, at a finite twist angle there is a momentum shift between the Dirac points, given by $|\vec{Q}| = K\theta$ for $\theta \ll 2\pi$. Thus equi-energy contours of the bottom and top layers are non-concentric circles, see Fig. 3(c). Upon tuning their relative energy eV_{KP} there are two situations where the Dirac cones are tangential,

$$eV_{KP} = \pm \hbar v_F \theta K \equiv \pm \Delta. \quad (19)$$

The calculated current with a finite twist angle of $\theta = 3.5^\circ$ is shown in the color plot of Fig. 5. We can

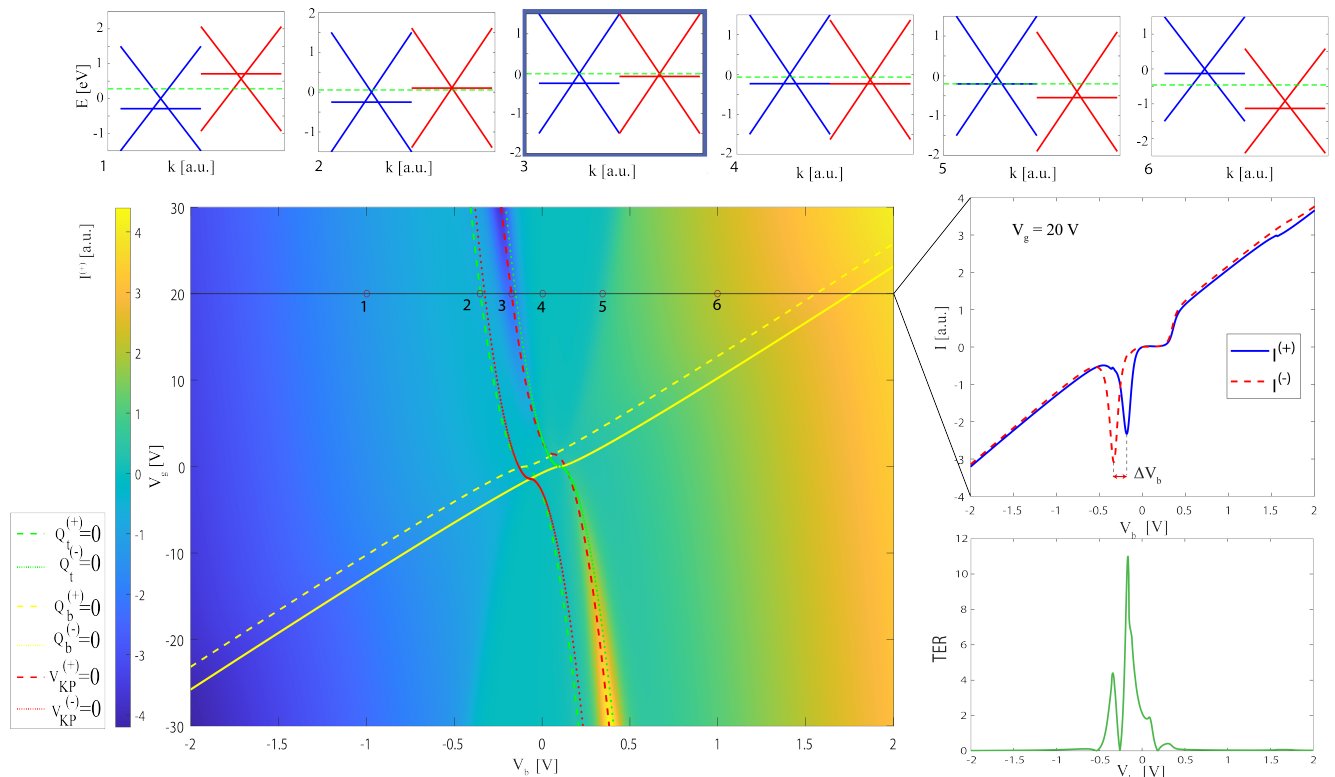


FIG. 4. Color plot showcasing the calculated current $I^{(+)}$ for one orientation ($p = +1$) of the polarization, as a function of the gate and bias voltage, for the untwisted case $\theta = 0$. On top of it are overlaid the curves for which the top and/or the bottom graphene electrodes are at the Dirac point (green $Q_t^{(+)} = 0$ and yellow $Q_b^{(p)} = 0$ curves, respectively), as well as the curves where the graphene sheets are electrostatically aligned (red curve, $V_{KP}^{(p)} = 0$). The right inset shows a cut of the $I - V$ curve at $V_g = 20V$ for both $p = \pm 1$. The two resonance peaks match with the band alignment condition $V_{KP}^{(\pm)} = 0$ and their line shape is given by Eq. (16). The top inset displays the Dirac bands (horizontally shifted for clarity) for $p = 1$, for points 1-6 corresponding to $V_g = 20V$ and $V_b = -1, -0.35, -0.17, 0, 0.34, 1.0V$. The resonance case corresponds to point 3 (blue outline). The green dashed lines represent the energy midway between the two Dirac points, at which the tunneling process conserves momentum. Tunneling through this energy state begins at point 5, at which the plateau in the right inset ends.

clearly see that the pair of resonance peaks, also shown along a cut of fixed gate, overlaps with the condition Eq. (19). The corresponding dispersion relations are shown in the top insets of Fig. 5. The sensitivity of the resonant peaks to different orientation of the polarization can be enhanced by tuning the gate such that the resonance peaks will occur near the charge neutrality condition of one graphene sheet. This is indeed seen for the cut of the $I(V_b)$ curve at $V_g = 9.5V$.

C. Dependence on G-G twist angle

We now discuss the twist-angle dependence of the resonance peaks. At $\theta = 0$ we observed a resonance peak whose position $V_{b,\text{peak}}^{(p)}$ depends on the polarization orientation $p = \pm$. The peak separation $\Delta V_b = |V_{b,\text{peak}}^{(+)} - V_{b,\text{peak}}^{(-)}|$ is a sensitive probe of the polarization, see Figs. 4 and 5.

The peak separation is plotted in Fig. 6 as a function

of V_g and θ . For zero twist angle we have seen in the inset of Fig. 4 that $\Delta V_b \sim 0.15V$ for $V_g = 20V$. We can see in Fig. 6 that at $\theta = 0$ this significant peak separation persists for any value of V_g , and peaks near $V_g = 0$. But at finite twist angle, the peak separation becomes visible only for specific values of V_g . For example for $\theta = 3.5^\circ$, as we have seen in the inset of Fig. 5, the peak separation is resolved only near $V_g \sim \pm 10V$. As discussed, this maximal sensitivity occurs when both Eq. (19) holds and one graphene sheet is at charge neutrality $Q_b = 0$. Therefore, in order to achieve good sensitivity in terms of resonance peak separation, one should operate such a device at specific twist angle dependent value of the gate voltage.

The slope of the high sensitivity spokes in the (V_g, θ) plane can be obtained analytically. By solving Eqs. (5) and (6), with the added condition of Eq. (19), we obtain the expression for the bias voltage at which the peak occurs as a function of V_g and θ . For a given twist angle, the difference of such bias voltage for the two orienta-

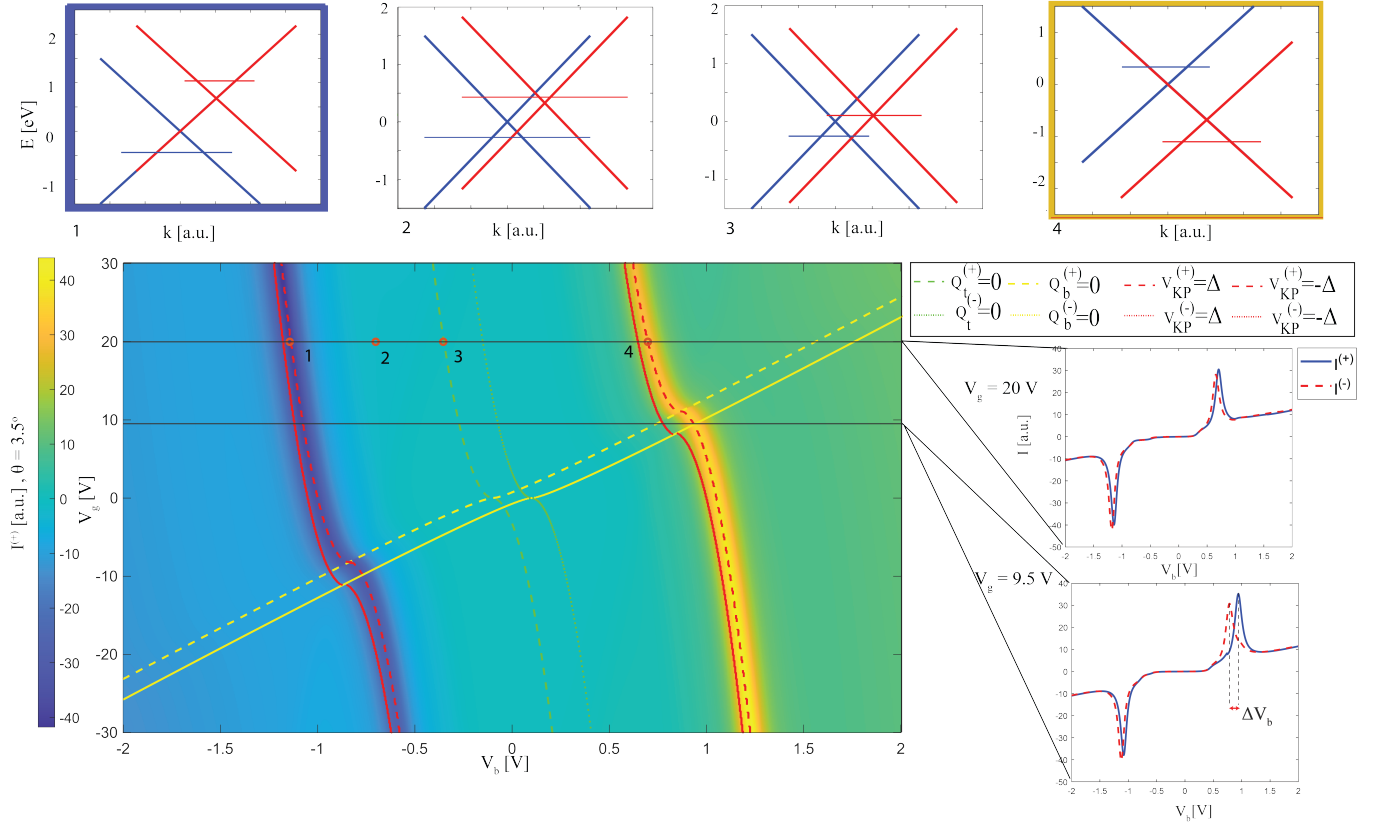


FIG. 5. Color plot showcasing the calculated current as a function of gate and bias voltage for specific orientation of the polarization ($p = +1$), with twist angle $\theta = 3.5^\circ$ between the graphene sheets. The resonance peak splitting to two peaks at $eV_{KP} = \pm\Delta$ is observed on the color plot. The right insets show two cuts at fixed gate voltages, plotting both $I^{(+)}$ and $I^{(-)}$. We can see that each peak of either $eV_{KP} = \Delta$ or $eV_{KP} = -\Delta$ further splits according to the direction of the polarization ($p = \pm 1$). The top inset shows the calculated band structure alignment (for points 1-4 corresponding to $V_g = 20\text{V}$ and $V_b = -1.14, -0.70, -0.35, 0.70\text{V}$).

tions of the polarization, representing the peak separation, is extremized analytically with respect to V_g . For large enough gate voltages (outside the range where both graphene sheets are near the charge neutrality), we find

$$V_g \simeq \pm \frac{C}{C_g} \frac{\hbar v_F}{e} K\theta, \quad (20)$$

which perfectly fits the spokes in Fig. 6 (not shown).

VI. SUMMARY

To summarize, in this work we studied graphene-FE-graphene junctions. We focused on the self-consistent interplay of the polarization with the electrostatics and quantum capacitance of the graphene electrodes. We first asked whether experiments will detect a polar domain voltage across the conducting graphene electrodes, and discovered that a finite signal appears only upon gate tuning of one of the Dirac electrodes to charge neutrality.

Moving to the tunneling current, we studied two mechanisms for its dependence on the polarization direc-

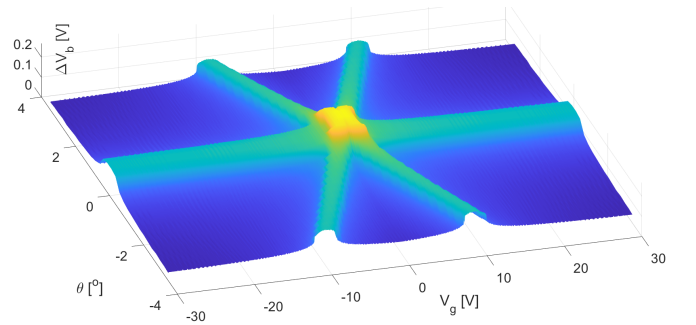


FIG. 6. Peak separation ΔV_b as function of gate voltage and twist angle θ . The peak separation is defined from the $I(V)$ characteristics as in the bottom inset of Fig. 5. For each V_g and θ , ΔV_b is the largest among the two peak separations.

tion. First, we discussed a dependence of the tunneling coefficient on the polarization. This barrier sensitivity becomes sizable upon increasing the bias voltage which leads to a device asymmetry, but is relatively small at zero bias for available values of gate voltages. We then considered 2D momentum conserving tunnel-

ing, and showed that one can detect the actual value of the polarization via a shift in the voltage axis of a resonant peak occurring in the $I(V)$ characteristics due to the alignment of the Dirac cones. This resulted in a sizable TER.

In order to switch from one state to the other, one would need, in practice, to slide a domain wall separating AB and BA stacking through the tunneling region. This could be achieved by tuning the bias V_b above the switching point. This process goes beyond the presented model.

Our results apply to Moiré superlattice materials such

as transition metal dichalcogenides. We hope that our theory will serve as a basis for analysis of near-future FE tunneling experiments.

VII. ACKNOWLEDGMENTS

We thank discussions with Moshe Ben Shalom, Igor Rozhansky, Simon Sallah Atri and Hadar Steinberg. This project received funding from the European Research Council (ERC) under the European Union’s Horizon 2020 research and innovation program under grant agreement No 951541.

-
- ¹ Lei Li and Menghao Wu, “Binary compound bilayer and multilayer with vertical polarizations: two-dimensional ferroelectrics, multiferroics, and nanogenerators,” *ACS nano* **11**, 6382–6388 (2017).
 - ² Kenji Yasuda, Xirui Wang, Kenji Watanabe, Takashi Taniguchi, and Pablo Jarillo-Herrero, “Stacking-engineered ferroelectricity in bilayer boron nitride,” *Science* **372**, 1458–1462 (2021).
 - ³ Maayan Stern Vizner, Yuval Waschitz, Wei Cao, Iftach Nevo, Kenji Watanabe, Takashi Taniguchi, Eran Sela, Michael Urbakh, Oded Hod, and Moshe Ben Shalom, “Interfacial ferroelectricity by van der waals sliding,” *Science* **372**, 142–1466 (2021).
 - ⁴ Astrid Weston, Eli G Castanon, Vladimir Enaldiev, Fabio Ferreira, Shubhadeep Bhattacharjee, Shuigang Xu, Héctor Corte-León, Zefei Wu, Nicholas Clark, Alex Summerfield, *et al.*, “Interfacial ferroelectricity in marginally twisted 2d semiconductors,” *Nat. Nanotechnol.*, 1–6 (2022).
 - ⁵ Sergio C de la Barrera, Qingrui Cao, Yang Gao, Yuan Gao, Vineetha S Bheemarasetty, Jiaqiang Yan, David G Mandrus, Wenguang Zhu, Di Xiao, and Benjamin M Hunt, “Direct measurement of ferroelectric polarization in a tunable semimetal,” *Nat. Commun.* **12**, 1–9 (2021).
 - ⁶ Swarup Deb, Wei Cao, Noam Raab, Kenji Watanabe, Takashi Taniguchi, Moshe Goldstein, Leor Kronik, Michael Urbakh, Oded Hod, and Moshe Ben Shalom, “Cumulative polarization coexisting with conductivity at interfacial ferroelectrics,” (2022), [10.48550/ARXIV.2206.12215](https://doi.org/10.48550/ARXIV.2206.12215).
 - ⁷ Menghao Wu and Ju Li, “Sliding ferroelectricity in 2d van der waals materials: Related physics and future opportunities,” *Proc. Natl. Acad. Sci. U.S.A.* **118**, e2115703118 (2021).
 - ⁸ Tingting Zhong, Yangyang Ren, Zhuhua Zhang, Jinhua Gao, and Menghao Wu, “Sliding ferroelectricity in two-dimensional moa 2 n 4 (a= si or ge) bilayers: high polarizations and moiré potentials,” *J. Mater. Chem A* **9**, 19659–19663 (2021).
 - ⁹ Daniel Bennett, “Theory of polar domains in moiré heterostructures,” *Phys. Rev. B* **105**, 235445 (2022).
 - ¹⁰ Daniel Bennett and Benjamin Remez, “On electrically tunable stacking domains and ferroelectricity in moiré superlattices,” *NPJ 2D Mater. Appl.* **6** (2022), [10.1038/s41699-021-00281-6](https://doi.org/10.1038/s41699-021-00281-6).
 - ¹¹ Daniel Pantel and Marin Alexe, “Electroresistance effects in ferroelectric tunnel barriers,” *Phys. Rev. B* **82**, 134105 (2010).
 - ¹² Vincent Garcia and Manuel Bibes, “Ferroelectric tunnel junctions for information storage and processing,” *Nat. Commun.* **5**, 1–12 (2014).
 - ¹³ LL Tao and J Wang, “Ferroelectricity and tunneling electroresistance effect driven by asymmetric polar interfaces in all-oxide ferroelectric tunnel junctions,” *Appl. Phys. Lett.* **108**, 062903 (2016).
 - ¹⁴ Lili Kang, Peng Jiang, Hua Hao, Yanhong Zhou, Xiaohong Zheng, Lei Zhang, and Zhi Zeng, “Giant tunneling electroresistance in two-dimensional ferroelectric tunnel junctions with out-of-plane ferroelectric polarization,” *Phys. Rev. B* **101**, 014105 (2020).
 - ¹⁵ Zhi Yan, Zeyu Li, Yulei Han, Zhenhua Qiao, and Xiaohong Xu, “Giant tunneling magnetoresistance and electroresistance in α - in 2 se 3-based van der waals multiferroic tunnel junctions,” *Phys. Rev. B* **105**, 075423 (2022).
 - ¹⁶ Jie Yang, Jun Zhou, Jing Lu, Zhaochu Luo, Jinbo Yang, and Lei Shen, “Sliding ferroelectric tunnel junctions,” *arXiv:2112.02886* (2021).
 - ¹⁷ James P. Eisenstein, Thomas J. Gramila, Loren N. Pfeiffer, and K. W. West, “Probing a two-dimensional fermi surface by tunneling,” *Phys. Rev. B* **44**, 6511–6514 (1991).
 - ¹⁸ James P. Eisenstein, Loren N Pfeiffer, and KW West, “Coulomb barrier to tunneling between parallel two-dimensional electron systems,” *Phys. Rev. Lett.* **69**, 3804 (1992).
 - ¹⁹ L. Britnell, R. V. Gorbachev, A. K. Geim, L. A. Ponomarenko, A. Mishchenko, M. T. Greenaway, T. M. Fromhold, K. S. Novoselov, and L. Eaves, “Resonant tunnelling and negative differential conductance in graphene transistors,” *Nat. Commun.* **4** (2013), [10.1038/ncomms2817](https://doi.org/10.1038/ncomms2817).
 - ²⁰ Artem Mishchenko, JS Tu, Y Cao, Roman V Gorbachev, JR Wallbank, MT Greenaway, VE Morozov, SV Morozov, MJ Zhu, SL Wong, *et al.*, “Twist-controlled resonant tunnelling in graphene/boron nitride/graphene heterostructures,” *Nat. Nanotechnol.* **9**, 808–813 (2014).
 - ²¹ Julian Chen, *Introduction to Scanning Tunneling Microscopy*, 3rd ed. (Oxford University Press, 2021).
 - ²² Zhi Yan, Xin Jia, Xiaowen Shi, Xinlong Dong, and Xiaohong Xu, “Barrier-dependent electronic transport properties in two-dimensional mnbi2te4-based van der waals

- magnetic tunnel junctions,” *Appl. Phys. Lett.* **118**, 223503 (2021).
- ²³ Zhi Yan, Ruiqiang Zhang, Xinlong Dong, Shifei Qi, and Xiaohong Xu, “Significant tunneling magnetoresistance and excellent spin filtering effect in cri 3-based van der waals magnetic tunnel junctions,” *Phys. Chem. Chem. Phys.* **22**, 14773–14780 (2020).
- ²⁴ M Ye Zhuravlev, Renat F Sabirianov, SS Jaswal, and Evgeny Y Tsymbal, “Giant electroresistance in ferroelectric tunnel junctions,” *Phys. Rev. Lett.* **94**, 246802 (2005).
- ²⁵ G Gerra, AK Tagantsev, and N Setter, “Ferroelectricity in asymmetric metal-ferroelectric-metal heterostructures: a combined first-principles–phenomenological approach,” *Phys. Rev. Lett.* **98**, 207601 (2007).
- ²⁶ Luis Brey, “Coherent tunneling and negative differential conductivity in a graphene/*h*-bn/graphene heterostructure,” *Phys. Rev. Appl.* **2**, 014003 (2014).
- ²⁷ Lukas Rogée, Lvjin Wang, Yi Zhang, Songhua Cai, Peng Wang, Manish Chhowalla, Wei Ji, and Shu Ping Lau, “Ferroelectricity in untwisted heterobilayers of transition metal dichalcogenides,” *Science* **376**, 973–978 (2022).
- ²⁸ Randall M Feenstra, Debdeep Jena, and Gong Gu, “Single-particle tunneling in doped graphene-insulator-graphene junctions,” *J. Appl. Phys.* **111**, 043711 (2012).
- ²⁹ Jiangbin Wu, Hung-Yu Chen, Ning Yang, Jun Cao, Xiaodong Yan, Fanxin Liu, Qibin Sun, Xi Ling, Jing Guo, and Han Wang, “High tunnelling electroresistance in a ferroelectric van der waals heterojunction via giant barrier height modulation,” *Nat. Electron.* **3**, 466–472 (2020).
- ³⁰ Sergio C de la Barrera, Qin Gao, and Randall M Feenstra, “Theory of graphene–insulator–graphene tunnel junctions,” *J. Vac. Sci. Technol B* **32**, 04E101 (2014).
-